LRP 558/96 October 1996

Papers presented at the

19th Symposium on Fusion Technology
S O F T

September 16-20, 1996
Lisbon, Portugal

Modified

LIST OF CONTENTS

LIST OF CONTENTS

DESIGN AND OPERATION OF THE POWER INSTALLATION FOR THE TCV ECR ADDITIONAL HEATING

D.Fasel, J. Alex*, A. Favre, T. Goodman, M. Henderson, P-F. Isoz, A. Perez, M-Q. Tran

Centre de Recherches en Physique des Plasmas, Association Euratom - Confédération Suisse
Ecole Polytechnique Fédérale de Lausanne, PPB, CH - 1015 Lausanne, Switzerland

*Thomcast AG, CH-5300 Türgi, Switzerland

Following a brief introduction to the TCV project, this paper concentrates on the **R**egulated **H**igh **V**oltage **P**ower **S**upply (RHVPS) system chosen to supply the nine gyrotrons, distributed in three clusters, that will deliver 4.5 MW of **E**lectron **C**yclotron **R**esonance **H**eating (ECRH) to TCV plasmas. The configuration of these clusters is described in some detail, including the results of site test both with dummy load (80 kV, 85 A, 2 sec) and the gyrotrons themselves (70 kV, 25 A, 2 sec). Some details are also given of gyrotron auxiliaries, interlock circuitry, control and data acquisition, and integration into TCV control environment.

1. INTRODUCTION

The TCV tokamak (**T**okamak à **C**onfiguration **V**ariable) has been in operation since November 1992. A large number of plasma shapes have already been produced and experiments with fast internal stabilisation coils are presently underway in order to reach the maximum design elongation of κ=3. **ECRH** has been chosen as additional heating system for TCV and its implementation is progressing in parallel with TCV operation. The system comprises **6** gyrotrons of the **diode** type at **82 GHz** (2nd harmonic) and **3** gyrotrons of the **triode** type at **118 GHz** (3rd harmonic). The total power delivered by the gyrotrons to the plasma will be **4.5 MW** for two seconds. The gyrotrons are grouped in three clusters, with each cluster fed by its own power supply. At present, two power supplies have been installed, but only one is completely tested. The third is under study in order to match the specific requirements of the triode gyrotrons.

2. TCV ELECTRICAL NETWORK

Figure 1 illustrates the additional systems designed to feed the power supplies foreseen for the TCV ECRH project together with the internal coil **F**ast **P**ower **S**upply (FPS) described in [3]. A description of the main tokamak electrical network may be found in [2]. Electrical power supply to the TCV systems may be derived from either of two sources :

		Alternator	50 Hz network
Pcc	[MVA]	1160	130
f	[Hz]	120 - 96	50
Un	[kV]	0 - 10	20
Sn*	[MVA]	220	7

*Pulsed

2.1 The 50 Hz network

The RHVPS may be directly supplied by the 20 kV grid through a pulsed transformer (named *Test*), also used in other applications (eq TCV rectifier tests, FPS tests).

There are several reasons why the gyrotron clusters should be fed in this way :

- to increase the short circuit impedance
- to ensure lower current (and hence increased installation protection) in case of short circuit
- to work independently with any cluster for conditioning purposes

In order to reach the required 10 kV at the primary side of the RHVPS, an auto-transformer with a voltage ratio of 1÷2 is used. The power rating of both this and the *Test* transformer allows us to work with a complete cluster at the maximum value, of **7 MVA** for **2 sec every 5 min**. This must, however, not be performed simultaneously with a TCV shot in order to avoid too much power being extracted from the grid. The three phase AC cable (1x3x95 mm²) used to feed all the equipment is chained from one isolator unit to another from the *Test* transformer secondary.

2.1 The generator network

Compared to the 50 Hz network, the TCV generator network differs in several respects :

- the working mode : pulsed with a duty cycle of 2 sec every 5 min
- the higher frequency (120 Hz)
- the 10 times higher short circuit power

In addition separate cables supply rectifier groups, FPS and the 3 gyrotron clusters from the generator busbars to the isolator units (see figure 1).

Using the alternator power source, the RHVPS power modules are active only at relatively low duty cycle, so thermal stresses are lower than at 50 Hz. Since the voltage is ramped up in 2 sec, the mechanical stresses in the RHVPS transformer are also lower.

3. THE CLUSTER STRUCTURE

3.1 General description

Shown in figure 1, each cluster comprises a power supply feeding three gyrotrons in parallel.

Three manually switched copper connections can either be tied to a **M**atching **N**etwork (MN) or to ground. The MN are used to adapt the line impedances to the fast voltage transients which appear, for example, during gyrotron arcing. A separate device places the two RHVPS output polarities to ground in the case of intervention inside the high voltage enclosure. A *triax* cable is used

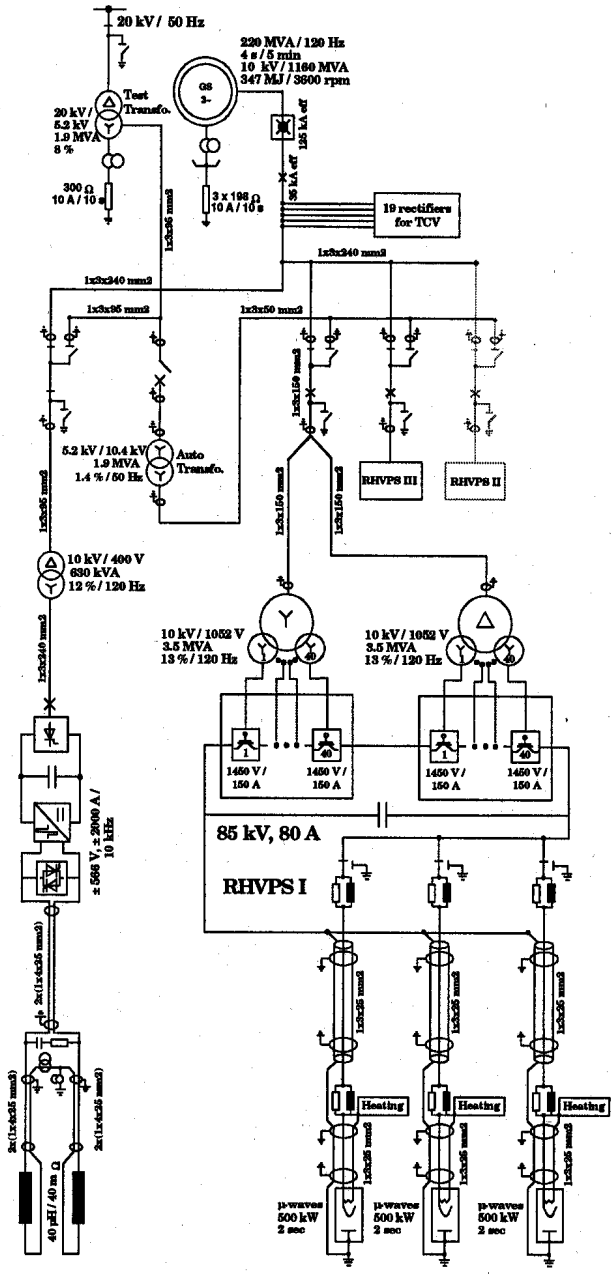

Figure 1 : Part of the TCV power supply

to connect each RHVPS output to the gyrotron cathode filament heating assembly. A *three conductor HV cable* then connects this equipment to the gyrotron.

As illustrated schematically in figure 2, the equipment is distributed physically on three floor levels.

3.2 Heating assembly

This assembly, which is referenced to the cathode potential includes :

- An MN connected to the *triax* cable central conductor
- The power components required to generate the current needed to heat the gyrotron cathode filament
- A control rack including :

- feedback electronics used to attain the current reference and to maintain this value in the range of ± **0.5%** of the demand value.

- fibre optic bus for communication with the main control system

- filament current and voltage measurements

- cathode current measurement

- A high voltage transformer supplying the heating equipment and isolated to 150 kV from ground

In order to improve shielding against fast transients, the electronics are located in a PerAluman (AlMg) enclosure.

3.3 Grounding configuration

The *power* ground is provided by copper bars or wires distributed all around the high voltage equipment in the RHVPS room. This network is referenced to building earth at several points on the grid.

On the AC side, a copper bar follows the power cables up to the *Test* transformer or the generator building in order to ensure a direct (low impedance) connection in case of a fault occur (eq short circuit). All the AC components (feeders, breakers, metallic pieces) are referenced to these bars.

On the DC side, the *triax* cable shield and the *3 conductor HV cable* are connected through a wire to the *power* ground.

On the level +1, where the gyrotron towers and control frames are located, the total floor surface is covered by a copper band mesh, both to minimise the high frequency impedance of this ground reference and to ensure personnel safety (this is an unrestricted access area) even during fast transients.

Since the gyrotron collector is at the same potential as the tower **and** the "+" RHVPS polarity, there are two grounding possibilities :

- leave the "+" polarity floating and reference the DC part to earth potential via the ground surface described above.
- leave the ground surface floating and reference it to earth via the "+" polarity connected to the *power* ground inside the RHVPS enclosure.

3.4 Triode particularities

The main differences are related to the additional power supply required to feed the gyrotron anode. It has to be placed as close as possible to the gyrotron tower in order to minimise the capacitative leakage. In the existing structure, possible locations are

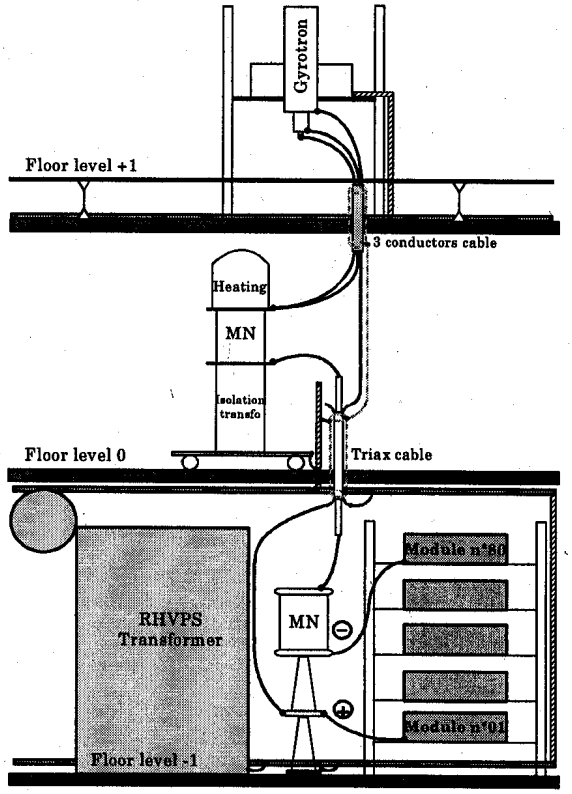

Figure 2 : Physical distribution of the gyrotron system

either under the gyrotron tower, or on an additional stage of the heating system (see fig.2)

The HV power supply needed to feed the triode cluster (118 GHz) is presently under study; the requirements are similar to those defined for the 82 GHz gyrotrons, except for the interface to drive the gyrotron anode power supply.

Although the cathode voltage is common to the cluster, the triode will permit independent modulation of the total microwave power using each anode supply.

3.5 Control

All gyrotron auxiliary systems are controlled and driven by distributed CPU nodes (named *slaves*), linked together through the BITBUS fieldbus, described in [4] and used for all TCV plant control.

The different *slave* tasks are:

- for the cooling: control of the pump status and the flow rate in pipes
- for the heating: ON/OFF orders, transfer of I/U cathode filament measurements, current reference, status of the gyrotron heating system
- for the control: centralise warnings and send related orders to the RHVPS and/or to the auxiliaries (pumps, magnetic field etc.), based on programmable logic. Convert fibre optic signals in TTL signals for arc detection on the window, **M**atching **O**ptical **U**nit (MOU) and that part of the waveguide transmission line which is not located in the TCV zone.
- for the pump : control of the waveguide vacuum.

Depending on the necessary tasks, *slaves* are dedicated to individual gyrotrons, a whole cluster or to the complete installation.

Data storage, visualisation, driving orders and parameter settings, have already been integrated into the TCV control system in order to minimise the effort required when microwave power is first injected into TCV plasmas.

4. RESULTS

4.1 Dummy load tests

On site commissioning tests have been performed using a resistive load (1060 Ω, 80A, 100 kV), to simulate the gyrotron environment as closely as possible: same cables, MN and grounding system.

Particular care has been taken with respect to requirements, such as :

- the ripple, which must be $< \pm$ **0.5 %** of the nominal HV DC. This requirement is satisfied by the use of an additional capacitor (15 nF) at the power supply output.
- the short circuit energy dissipation, which must be **< 10 J**. A *Cu wire* test showed that this requirement is also satisfied.

The ability to work in pulsed mode with the motor generator has also been tested. The main difference here lies in the power-up time of the power module forming the RHVPS : using the generator, the voltage ramp-up time is less than 2 sec. After this time, the voltage supply for the power module must be stabilised and the electronics alive and ready to work.

4.2 Gyrotron tests

To date, gyrotron tests are performed only with the 50 Hz power source and with a single gyrotron connected to the RHVPS (see figure 4).

The biggest difficulties were encountered during the gyrotron conditioning period. When arcs occured either in the gyrotron cavity or in the MOU/transmission line. As a consequence perturbations were observed on the control or heating electronics, strong enough in some cases to interrupt some differential inputs and terminate operation. To minimise such perturbations, the grounding configuration has been modified:

- reference the "+" polarity of the RHVPS to the *power* ground in the HV enclosure.

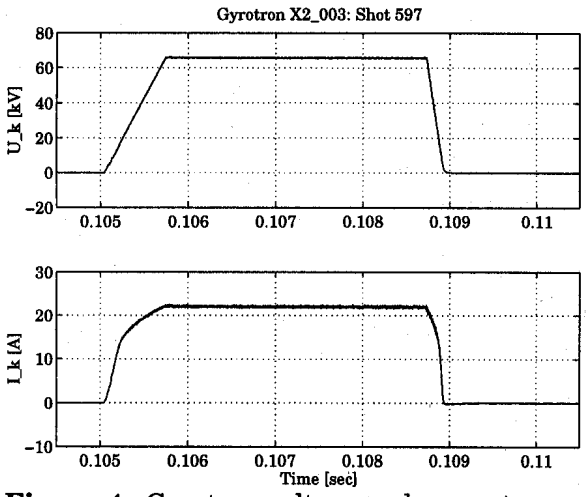

Figure 4 : Gyrotron voltage and current

- reference the copper earth mesh to the "+" polarity through the cable shields
- adapt the gyrotron tower connection to the copper earth mesh, replacing the wire connections by copper band.

Signal cables directly connected to gyrotrons (such as the gun and collector currents and pressure measurement) have also been protected with fast varistors in parallel with a surge voltage limiter. In addition, a copper shield has been installed around the gyrotron coils (gun, collector) to decrease the antenna effect during fast voltage transients.

4.3 RHVPS improvements

Operation with the 50 Hz network has suggested a number of possible improvements to the RHVPS. The most important are:

- the IGBT driver exchange on the power module board. The original driver was being influenced by voltage transients through the galvanic isolation transformers. This problem is now avoided through the use of an optical coupling.
- Due to a new requirement on the permitted energy dissipation in the gyrotron during an arc (**5 J** instead of 10 J **specified**) the inductive stored energy has been decreased by the addition of diodes in parallel with the RL filter in series with each power module.

5 CONCLUSION AND FUTURE PLANS

At present, a single RHVPS is in use, feeding a cluster of 3 gyrotrons of which only one is currently operational. Continuous testing of the unit on the 50 Hz network has demonstrated the ability of this supply to wishtand the gyrotron operation environment. Full power operation for 2 sec at 500 kW gyrotron output power, injected into a waveguide transmission line right up to TCV tokamak, has been obtained

The next step will be to operate the RHVPS from the generator power source, firing microwave power into a dummy load at TCV. Later tests will be performed with the RHVPS supplying a complete cluster in order to investigate the mutual influence of 3 gyrotrons fed by a common power source.

In 1997, tests of the second cluster and the installation of the third RHVPS for supply of the 118 GHz triodes are foreseen . In parallel, delivery and commissioning of the anode power supplies will take place.

REFERENCES

[1] G. Besson et al., Regulated high voltage power supply for gyrotrons based on pulsed step modulator technology, SOFT 1994, vol.1, p.517-520

[2] D. Fasel et al., 19 rectifiers to supply the coils of the TCV tokamak, SOFT 1990, vol.2, p.1492-1496

[3] A. Favre et al., Control of highly vertically unstable Plasmas in TCV ..., this volume

[4] JB. Lister et al., Distributed on the TCV tokamak and modular bitbus nodes, SOFT 1990, vol.2, p. 1268-1272

This project is partly supported by Swiss National Science Foundation

Control of highly vertically unstable Plasmas in TCV with internal Coils and Fast Power Supply

A. Favre, J.-M. Moret, R. Chavan, A. Elkjær*, D. Fasel, F. Hofmann, J.B. Lister, J.-M. Mayor, A. Perez

CENTRE DE RECHERCHES EN PHYSIQUE DES PLASMAS
Association EURATOM - Confédération Suisse,
Ecole Polytechnique Fédérale de Lausanne, UHD-PPB, CH - 1015 LAUSANNE, Switzerland

* Danfysik A/S, DK - 4040 Jyllinge, Denmark

The goal of TCV (Tokamak à Configuration Variable) is to investigate effects of plasma shape, in particular high elongation (up to 3), on tokamak physics. Such elongated configurations ($I_p \cong 1$ MA) are highly vertically unstable with growth rates up to $\gamma = 4000\ s^{-1}$. Control of the vertical position using the poloidal coils located outside the vessel is limited to $\gamma \leq 1000\ s^{-1}$ because of the shielding effect of the conductive vessel and because of the relative slow time response of their power supplies (0.8 ms thyristor 12 pulse switching at 120 Hz). This dictated the necessity to install a coil set inside the vacuum vessel fed with a **F**ast **P**ower **S**upply (FPS).

The choice and design of the system with a special attention to the mechanical and electrical constraints in TCV tokamak, as the results and real performances, will be presented.

1. FAST INTERNAL COIL

The fast internal coil is made of two sets of three toroidal turns located in each outer corner of the vacuum vessel (G coil in figure 1.1). Their exact position results from a trade-off between mechanical design constraints and a maximum wall separation to reduce field screening by image currents in the conductive vessel. Both coil sets are connected in anti-series to create a radial magnetic field at the plasma location. The nominal current (2 kA) was chosen such that this radial filed can restore a 1cm shift in the vertical position [2]. The rated voltage is such that this current can be established faster than the vertical instability growth rate (250 μs).

Vertical disruption or disruption of non up-down symmetric configuration has been estimated to induce currents of about 2 to 15 kA in the fast internal coil, depending on the total resistance of the coil itself, the transmission line and the crowbar internal resistance. These currents lead, in the poloidal magnetic field, to a force of about 100 to 200 kN per turn in the fast internal coil.

Figure 1.1
TCV Tokamak

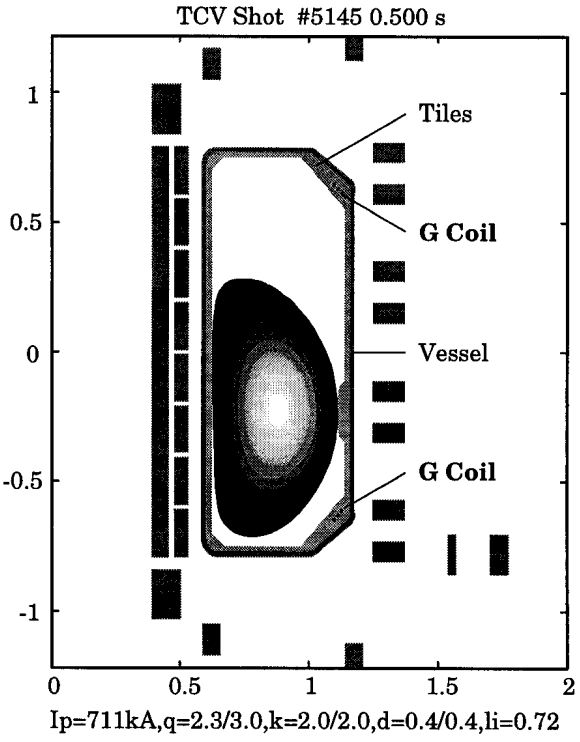

Figure 1.2
Feed Through

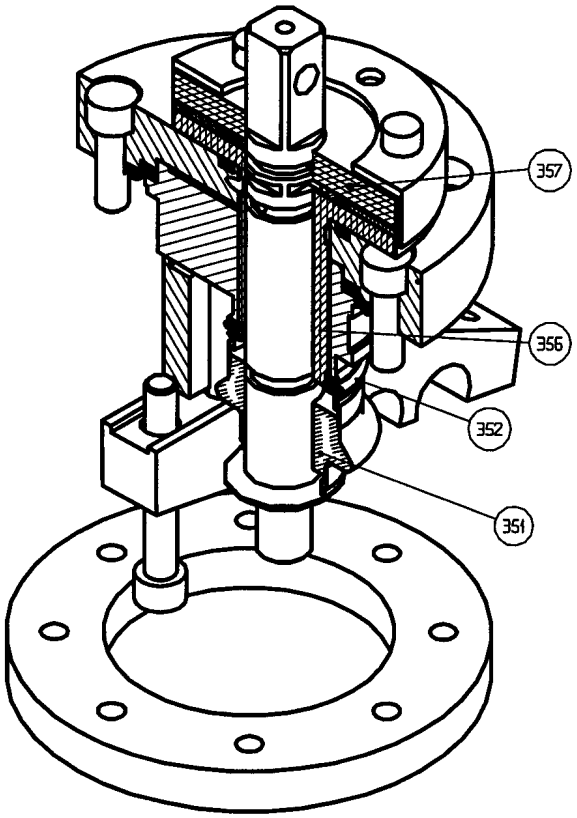

The windings are made of 10 mm diameter non insulated copper bars held in 48 ceramic rings per turn and protected from direct plasma exposure by graphite tiles (see figure 1.1). In practice, each turn is divided in four quarters for easier installation and to have the possibility for controlling non axisymetric perturbations with four independent power supplies. Quarters are connected with flexible parts having the form of two turn springs to compensate thermal expansion of the conducting bar (3 mm per quarter at 350° C). Special attention has been given to the current feed through, whose design is sketched in figure 1.2. In this design, the problem of the forces on the conductor and of the vacuum have been separated. In figure 1.2, parts #356 and #357, made of Pamitherm, ensure the mechanical rigidity of the system, while the brased ceramic #351 ensures vacuum. This fragile piece is mechanically decoupled with a bellow #352. The whole system is air-cooled to protect the insulation material of the connected transmission line during baking of the vacuum vessel. The internal coil main parameters are listed in table 1.3.

Table 1.3
Coils Parameters

Parameter	Value
Coil Impedance (frequency dependent)	40 μH to 100 μH 10 mΩ to 100 mΩ
Coil Current (plasma disruption)	15 kA - 10 MA^2s (Coil short-circuited)
Coil Voltage (plasma disruption)	2 kV (Coil in open circuit)

2. POWER SUPPLY DESIGN

Considering that the poloidal field system is able to take over the plasma vertical control after a few ms, it has been decided to choose a non-linear (switching mode) power supply and to specify it in terms of voltage reaction time and current controllability rather in terms of bandwidth and accuracy.

The main difficulties concerns the low inductance of the load and the high constraints caused by plasma disruptions. This has dictated the whole power supply design.

The selected structure [1] consists of two main elements, the *DC Power Source* which produces the regulated DC voltage and the *Fast Output Stage* which is able to apply the fast voltage pulses to the load.

The DC Power Source is constituted of a controllable *Thyristor Rectifier* (block 6 of figure 2.1) able to adapt the Fast Output Stage output voltage envelop during the plasma discharge. A damped *R-L-C DC Filter* (block 7) is placed at DC output to limit the voltage ripple and to provide fast current pulse to the Fast Output Stage. It is constituted of two capacitor banks, damping resistors and the leakage inductance of the Infeed Transformer. The *DC Chopper* (block

Figure 2.1
Power Supply Block Diagram

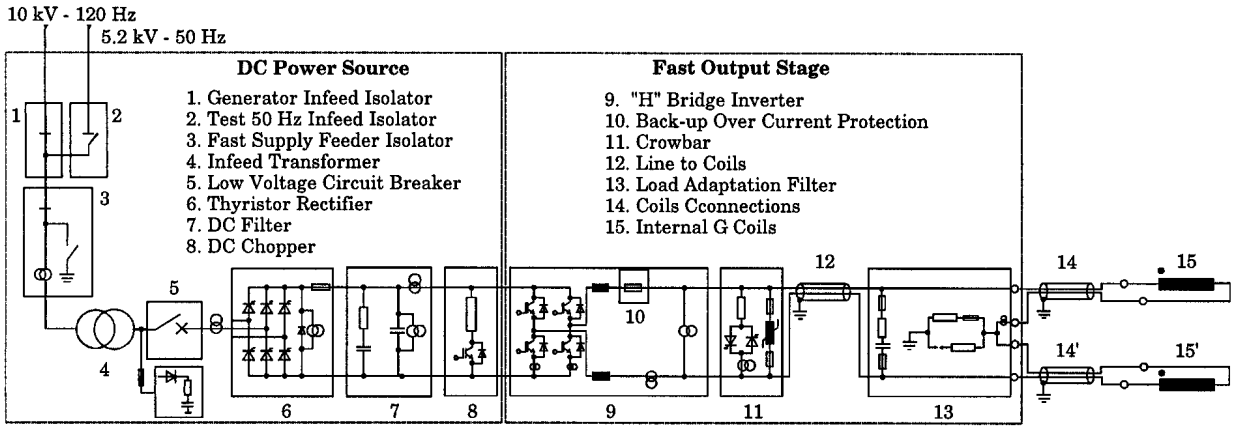

8), constituted of IGBTs in series with power resistors, is added for dissipation of the energy which can be reflected from plasma or other tokamak coils without output crowbar firing what would imply system loss of control.

Because three different possible output voltage levels has been found sufficient, the Fast Output Stage is composed of a single *H-Bridge IGBT Inverter*. This inverter (block 9 of figure 2.1), constituted of IGBT switches, is designed to be able to operate with a rated switching frequency of 10 kHz (up to 25 kHz) with voltage reaction time delay and minimum on time in the µs range. This is necessary for sufficient current control on the connected low inductance load. To protect the power supply against plasma disruption, a thyristor *Crowbar* (block 11), used as over-voltage and over-current protection device, is located at output, while a *Back-up Over Current Protection* (block 10) is added to avoid major damage in the case where all electronic over-current interlocks fail. A *Load Adaptation Filter* (block 13) is located near the tokamak coils. It include an RC filter acting as transmission line HF termination, the circuits necessary to refer the coil to ground and the terminals requested for serial connection of the two half coils. The Power Supply parameters are listed in table 2.2.

Table 2.2
Power Supply Parameters

Parameter	Value
Output Current	± 2000 A
Output no load Voltage	± 566 V
Current Rise Time	0.25 ms
Current Controllability	± 100 A at ±2000 A ±40 A at ±50 A
Voltage Reaction Time	5 µs
Switching Frequency:	10 kHz Typical 25 kHz Max.

The control electronics are based on a central microcomputer Control Board and especially designed modules for the control of each sub-part. The heart of the power supply electronics is constituted of the H-Bridge Control Module in which the control modes as the fast interlocks and sequences are implemented using Field Programmed Gate Array (FPGA) chips. The power supply can be used as a current source (double band hysteresis current regulator), as a voltage source (open loop voltage PWM modulator) or as a three levels voltage source (H-Bridge switches directly driven through digital signals). The H-Bridge and its drivers are fitted with fast short-circuit (IGBT de-saturation) and over-current (serial collector resistors) detectors which allow detection of an over-load (not only a short-circuit) in less than one µs. For fault detection and

diagnostic, the Power Supply is fitted with fast measurements (200 kHz range) for all AC / DC voltages and currents connected to TCV Data Acquisition System.

3. TCV PLANT IMPLEMENTATION

TCV plasma control is processed by an hybrid analog-digital matrix multiplier. For vertical control, the real-time position observer ($I_p \cdot z$), built upon tokamak magnetic probes, is used to provide FPS analog voltage or current reference as it is the case for poloidal field system.

With the implementation of the TCV Digital Plasma Control System, the control of the H-Bridge switches could be directly processed through a digital interface.

4. TESTS AND RESULTS

Because the real tokamak load is complex to modelize and the power supply exact requested output wave forms were not well known, it has been chosen to define and test performances with specified voltage and current *Reference Wave Forms,* the power supply being connected to a dummy load. After improvement to Fast Output Stage, performances better than requested has been reached. Figure 4.1 and 4.2 show examples of Reference Wave Forms obtained supplying the tokamak G coil set.

Low current plasmas has been first chosen to limit risks of system failure. Then elongation (κ) and as a consequence the growth rate (γ) has been progressively increased to tune the vertical position feedback corrector. Growth rate higher than never reached with poloidal field system only has been achieved in the first weeks of operation ($I_p = 250$ kA, $\kappa = 1.8$, $\gamma = 1700\ s^{-1}$). Progressive increase of plasma current and elongation will follow up to TCV rated parameter ($I_p = 1$ MA, $\kappa = 3$).

5. CONCLUSION

The possibility to implement a high stress withstand coil system and to adapt an industrial based and relative low cost power supply in a tokamak particular environment has been demonstrated. The efficiency and reliability of the whole system during TCV tokamak long term operation remain to be proved.

6. REFERENCES

1. A. Favre et al. Fast Power Supply for Vertical Stabilization of TCV Tokamak Plasmas, CERN EP2 Forum 95, Vol. ETG 43 e A15, 1995.
2. F. Hofmann, G. Tonetti et al. LRP 426/91, CRPP Lausanne, 1991.

The TCV Tokamak project is partly supported by Swiss National Science Foundation.

Figure 4.1

Power Supply PWM Voltage Control

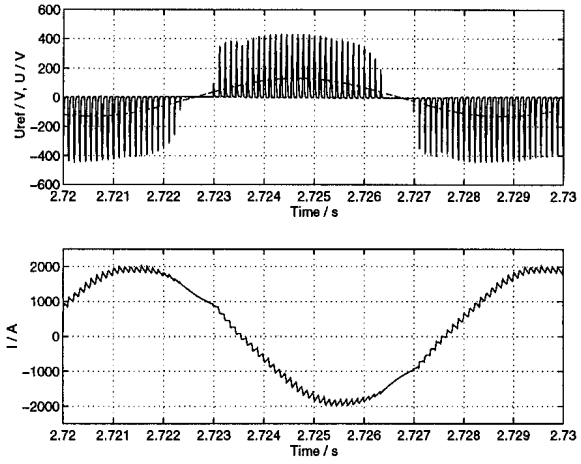

Figure 4.2

Power Supply Closed Loop Current Control

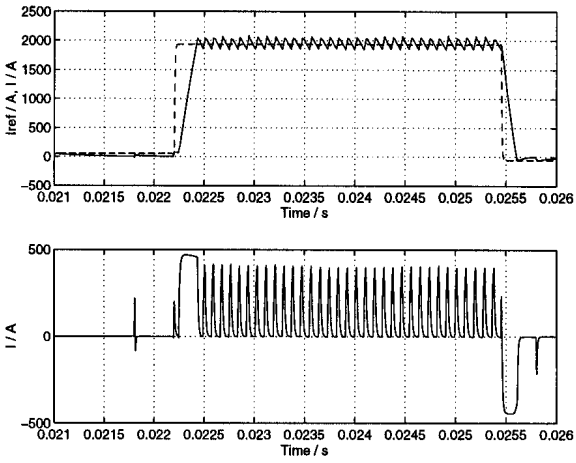

Modelling and engineering aspects of the plasma shape control in ITER

R. Albanese[(1)], G. Ambrosino[(1)], E. Coccorese[(1)], J.B. Lister[(2)], A. Pironti[(1)], D.J. Ward[(2)]

[(1)] Consorzio CREATE, Dipartimento di Ingegneria Elettrica, Universita di Napoli, Italy
[(2)] CRPP-EPFL, Association EURATOM-Suisse, 1015 Lausanne, Switzerland

As part of the ITER Engineering Design Activity, a number of questions related to plasma control has been addressed, using linearised and non-linear simulation codes to assess the control of the plasma shape given the particular design restrictions of ITER.

1. INTRODUCTION

Due to the size and consequent cost and power limitations of ITER, there will be less margin for plasma control than on current tokamaks and so particular attention is being addressed to the adequacy of the plasma control system. In this paper, we address several issues related to the Poloidal Field Control System, using and comparing two models, the TSC code [1] and a linearisation of PROTEUS [2].

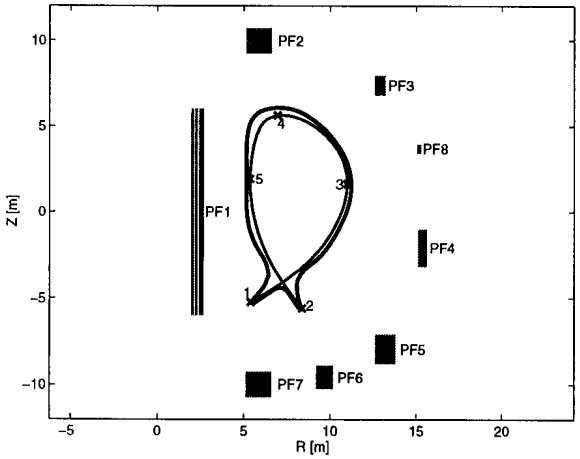

Figure 1. ITER PF coils, plasma facing wall contour, separatrix at End Of Burn and the 6 point separatrix-wall gaps used to define the plasma response.

TSC (Tokamak Simulation Code) is a two-dimensional time-dependent free-boundary MHD simulation code. Perturbed equilibrium calculations from the PROTEUS code are used to determine the non-rigid linearised plasma response to individual variations in conductor currents and to variations of βp and li, given some simple physical constraints on conserved quantities.It is important to verify that the latter model, well suited to the design of controllers and scoping studies of control techniques, agrees with the more physically complete former model. More complete details of this work can be found in [3].

2. MODEL COMPARISON

As a first test, a 1 second square voltage pulse was injected into the PF coils one at a time for the End-Of-Burn equilibrium, in the absence of shape or positional feedback. Figure 2(left) illustrates the case of PF7. The agreement between the two models is good both for the contour displacement seen in the figure and the PF coil currents, not shown.

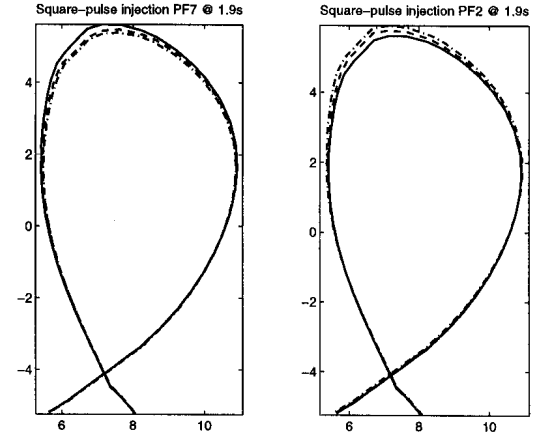

Figure 2. Injection of a square voltage pulse into PF7 (left) and PF2 (right). The TSC evolution of the separatrix-wall gap contour is shown as dashed lines and the linearised simulation is shown as dotted-dashed lines.

Figure 2(right) shows injection into the PF2 coil, with worse agreement, up to a factor of two between the peak contour displacements. The origins of this disagreement are being sought, particularly where it might stem from physical realities missing from the linear model, such as the induction of surface currents.

Secondly, we compare the open loop response of the separatrix to a plasma disturbance, namely $\Delta li = -0.1$ over 1 msec, subsequently evolved for 0.5 sec. Figure 3 compares the separatrix contours of the two models at 0.1 and 0.5 seconds after the disturbance. The initial displacement does not show perfect agreement, but the subsequent evolution agrees well. The PF currents show a significant discrepancy at 0.1 sec, with PF8 showing a sign difference and PF1 showing a significant difference in magnitude. The deformation of the complete contour shows reasonable agreement at the early time. At t = 0.5 sec, the evolution is more dependent on the passive structure dynamics and the agreement is good, for both the contour and the currents.

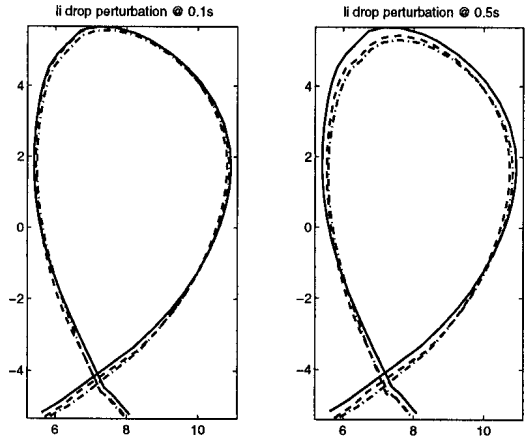

Figure 3. ITER disturbance response to $\Delta li = -0.1$ at t=0.1 sec (left); t=0.5 sec(right).

$\Delta\beta p = -0.2$, modelled in TSC by enhancing the anomalous thermal diffusion coefficient over 4 msec. again gave good agreement for the slow evolution, but the initial displacement is in less good agreement than the case of the li drop. PF8 and PF1 again show anomalous behaviour at the early time. At the later time, the PF currents are not too dissimilar, but the contour shows a significant departure. Combining a βp drop and li drop shows better agreement, the previous disagreements partially cancelling. Again, the reasons for the apparent disagreement are being sought. However, the overall agreement is considered to be excellent, justifying the use of the linearised model in the design of the controllers. Further comparisons will be required to confirm this optimism.

3. PLASMA DISTURBANCE REJECTION

A study was carried out to estimate the hypothetical best possible control of each gap in the presence of a particular disturbance, namely $\Delta\beta p = -0.2$ and $\Delta li = -0.1$. Fully saturated voltages are applied to all PF coils at the time of the disturbance, with each coil voltage chosen to reduce the excursion of that particular gap. This procedure was carried out one gap at a time. Since the system responds better than any real controller, this control is referred to as the "Best Achievable Single Gap Control" (BASGC) and derives a lower limit of the response to the disturbance given the voltage saturation limits. All other gaps are non-optimal and may even have the opposite sign of desired reaction to the disturbance. The task of a full controller is exactly that of finding a suitable compromise for all gaps.

Figure 4 illustrates the time evolution of a typical gap (# 3, Fig. 1) using this BASGC. The solid line is the gap displacement with voltage control and the dashed line is the open loop gap displacement. The control action only has a significant effect after the initial displacement has completed, after which the evolution with no control and with BASGC occur on the same timescale, that of penetration of the flux through the passive structure. Since the control action response grows slowly, the response amplitude is dominated by the disturbance response.

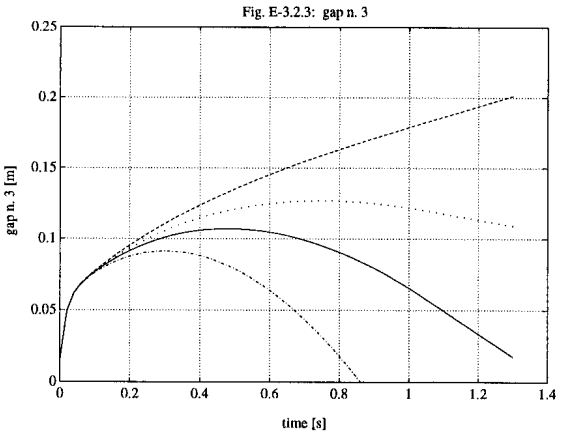

Figure 4. The evolution of gap # 3 following a disturbance given by $\Delta\beta p$ = -0.2 and Δli = -0.1.

Table 1. Performance of the "Best Achievable Single Gap Control" for all 5 gaps with the disturbance $\Delta\beta p$ = -0.2 and Δli = -0.1.

1	Excursion (cm)			Recovery (s)		
%	50	100	200	50	100	200
1	13.1	11.7	10.8	>2	1.2	0.7
2	7.8	7.5	7.2	>2	0.74	0.4
3	12.7	10.7	9.1	>2	1.28	0.8
4	12.0	8.7	7.0	1.8	0.88	0.5
5	11.2	6.3	4.	1.2	0.58	0.3

Halving the voltage limits, the gap displacement is only slightly worsened (dotted curves in Fig. 4). Doubling the voltage limits gives the dotted-dashed curves. The gap responses to this type of disturbance exceed the nominal specifications of the gap control, which should limit the displacement to 10 cm. The results of this analysis are summarised in Table 1, in which we list the gap numbering (Column 1), the maximum excursion (Column 2) and the time for the disturbance response to reduce to 2 cm (Column 3), both measurements assessed for 50%, 100% and 200%. of the nominal PF coil voltage limits. Although the excursion is not reduced much if the voltage is doubled, the recovery time is sensitive to the applied voltages. However, the recovery times with the nominal voltages are already more than adequate.

4. COIL VOLTAGE SATURATION

The most serious non-linearities in the plasma - passive structure - coils - power supply system are the voltage and current limitations of the power supplies themselves. The performance of any optimised controller is no longer guaranteed once the controller response reaches the power supply saturation. The performance of the closed loop will then depend sensitively on the amplitude of any disturbances or reference input changes. It is probable that the coil saturation presents more of a challenge to the controller design than the optimisation of the ideally linear closed loop. The problem of coil voltage saturation is likely to be much more severe in ITER than in present experiments in which it can be avoided by careful scenario programming to retain a sufficient voltage margin for control. The problem of current saturation in ITER will be identical to currently operating tokamaks.

Work has started on an approach in which the design of the controller explicitly considers the presence of coil voltage or current saturation, providing a modification to any A,B,C,D controller. The feedback error is adapted so that the controller outputs remain within the voltage and current saturation limits. Furthermore, the modification to the errors are chosen so that some of them are better respected than others, giving rise to the apellation "Hierarchical Saturation Controller". Any controller which has been designed to be optimal in a small signal sense can be handled, preserving as much of its functionality as possible in the presence of the saturation.

A plasma disturbance given by $\Delta\beta$ = -0.25 is illustrated in Figs. 5(a,b). The coil voltage saturation levels were taken as: [10, 16, 14, 15, 17, 10] Volts per turn for PF2-7. For each simulation the following evolutions are shown: a) the 6 gaps; b) the 6 PF coil voltages (PF1 and PF8 were not used); c) the corresponding 6 PF coil currents; d) the total power requirement.

Figure 5(a) illustrates the case of an optimised LQG controller without saturation compensation. The voltage saturation is seen at different times on several coils. The power requirement, shown in the lower figure as a line of crosses, exhibits both positive and negative surges while the voltage saturation occurs. The physical origin of this effect stems from the fact that the energy required to correct a change in beta-poloidal and the corresponding vertical displacement is rather modest. The controller output demand voltage reflects this. However, if the coil voltage saturates, this correction is wrong and the total energy injected during the initial correction is no longer small. Subsequently, the controller has to recover from this energy error, and the power demand is again excessive since this correction itself suffers from a voltage saturation and a further power excursion occurs.

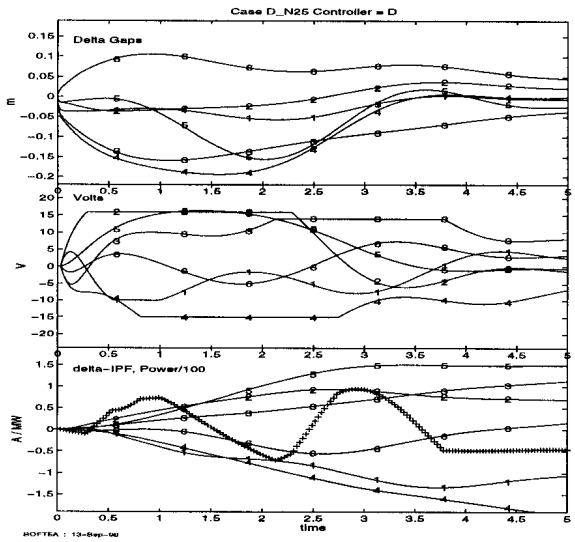

Figure 5(a). Control response without saturation correction.

Figure 5(b) shows the same disturbance, but with the saturation compensating controller in operation. Only a little improvement is found in the evolution of the gaps, and the voltage waveforms show a similar evolution, with trace 1 (PF2) no longer in saturation. Most noticeably, the power requirement has been reduced. Both simulations show asymptotic rejection of the disturbance. The uncompensated controller produced a PF power slew-rate which is outside the nominal specifications of the PF system, whereas the compensated controller had a barely noticeable power and power slew-rate requirement.

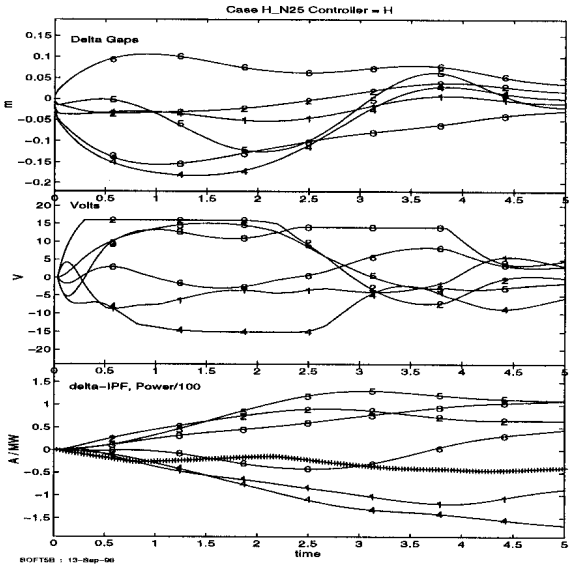

Figure 5(b). Control response with saturation correction.

Acknowledgement: This work was partly funded by NET Contracts. The authors thank to Fabio Villone and Parag Vyas for their help in the preparation of the paper.

REFERENCES

1. S.C. Jardin, N. Pomphrey, J. De Lucia, J. Comput. Phys., 66, 481(1986).
2. R. Albanese et al., Nuclear Fusion 29, 6 (1989)
3. J.B. Lister et al., Lausanne Report LRP 552/96 (1996)

Time resolved energy dispersive X-ray diagnostic for the TCV tokamak

J. Sousa[1], P. Amaro[1], P. Amorim[1], B. Duval[2] and C.A.F. Varandas[1]

[1] Associação EURATOM/IST, Centro de Fusão Nuclear,
Instituto Superior Técnico, 1096 Lisboa Codex, Portugal.

[2] Centre de Recherches en Physique des Plasmas, EPFL,
Association EURATOM/Confédération Suisse, 1015 Lausanne, Switzerland.

A time resolved energy dispersive X-ray diagnostic is being developed for the TCV tokamak (CRPP - Lausanne) to measure the evolution of the plasma impurities, runaway electrons and electron temperature. A liquid nitrogen cooled Ge diode detects the X-ray photons which are processed by a spectroscopic amplifier and a locally developed interface amplifier and timing generator (IATG) unit. The energy spectrum is obtained using a fast digitiser and a software histogramming algorithm. These electronics components have been optimised to improve the data throughput to match high flux 2 seconds time duration of a TCV plasma pulse. This paper describes the diagnostic hardware with particular emphasis on the IATG unit.

1. INTRODUCTION

Measurement of the X-ray spectrum by means of pulse height analysis is used nowadays by many tokamaks to identify the main high Z plasma impurities, to measure the electron temperature (T_e) and to detect the runaway electrons [1]. This paper describes an energy dispersive X-ray diagnostic that has been developed for the TCV tokamak [2] aiming at performing time resolved measurements in L and H mode regimes [3].

Section 2 contains the general description of the diagnostic, which is based on a liquid Nitrogen cooled solid state Germanium diode. This detector is sensitive to X-rays in the 1-100 keV range, with energy resolution of about 130 eV. Section 3 presents the specially developed electronic unit that is used to post-reconstruct a sequence of groups of X-ray events which arrive during periodic intervals of time. Section 4 describes the installation of the diagnostic on the TCV tokamak and section 5 includes the experimental results. Finally section 6 contains the conclusions and planned system enhancements.

2. GENERAL DESCRIPTION OF THE DIAGNOSTIC

A block diagram of the hardware is shown in Fig. 2. Each photon event generates a current pulse in a liquid Nitrogen cooled solid state Germanium diode (Canberra GUL0055P) which is pre-amplified (Canberra 2008) and further shaped by a gated integrator (GI) (ORTEC 673). Time coincident pulses that result in overestimated photon energies measurements (pileup) are detected and omitted from the output. The amplitude of the positive unipolar pulses is recorded by a CAMAC digitiser module (INCAA TRCH) which has 12 bits resolution, 1 Mega samples of memory and an 1 μs cycle time. The spectrum is determined by a software histogramming of the acquired pulse heights. The post-reconstruction of the arrival time of a group of events is permitted by a periodic (1-50 ms) negative time pulses of linear amplitude variation, added in the signal path,

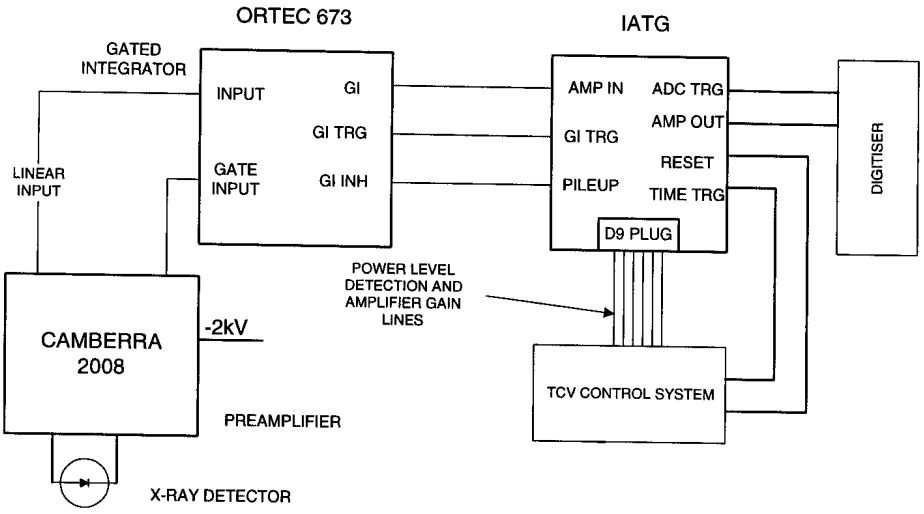

Fig. 2. Block diagram of the hardware setup.

by the dedicated electronic unit described in the next section.

3. INTERFACE AMPLIFIER AND TIMING GENERATOR MODULE

The specially developed interface amplifier and timing generator (IATG) module receives a programmable train of periodic pulses from the TCV timing system for generating the periodic time pulses. When a collision occurs between a signal pulse and a time pulse it discriminates them by delaying the second event for a time of 1 μs.

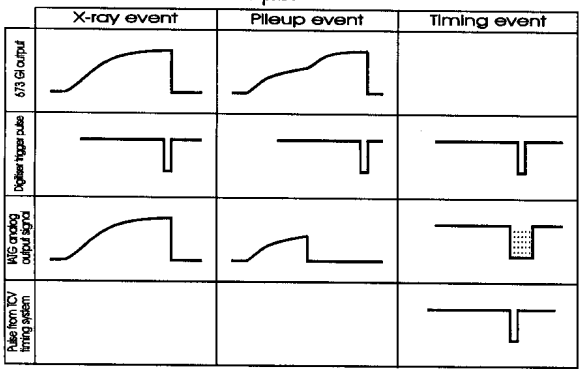

Fig. 1. Timing diagram of IATG.

The main requirements of this module are:

a) It should generate a pulse to trigger the digitiser whenever an event peak occurs. In Fig. 1, under the heading "X-ray event", is depicted the integrated event pulse at the GI output and the generated IATG trigger output.

b) Whenever a pulse pileup is reported by the gated integrator, the signal at the digitiser input should be zero. In Fig. 1, under the heading "Pile-up event", we can see the IATG output analog signal falling to zero immediately after the pileup occurrence .

c) It must output the time information that comes from the TCV timing system to the digitiser, in the form of a negative value which amplitude depends on its time position. This situation is depicted in Fig. 1, under the heading "Timing event".

d) It must prevent collision between time and event pulses by queuing them in two time slots of 1 μs. In this process an error of ±1 event pulse can occur for that spectrum, which is similar to the error of closing the gate in a multichannel analyser.

The IATG unit can be graphically represented as a group of interconnected functional blocks which is presented in Fig. 3.

The programmable gain amplifier (PGA) amplifies the event pulses that come from the GI output and can be set for gains of 1, 2, 4 and 8. Each pulse peak value is stored in an track and hold device (T&H) during a 1 μs

(single event) or 2 μs (when a pulse coincidence occurs) interval. The holding time is defined by the GIPULSE, HOLD1 and HOLD2 variables.

An analog multiplexer selects one of these three signals: stored event pulse (AGI), timing value and zero volt. The selection depends on the levels/transitions of the three signal sources: PILEUP, GIPULSE and TPULSE. The multiplexer output is connected to an analog buffer of low output impedance, driving loads down to 50 ohm. The output (ANLOUT) is then connected to the digitiser.

TPULSE comes from the TCV timing system and provides the clock for generating the timing values. Each time a transition occurs in this input, a binary counter (COUNTER) is incremented and a digital to analog converter (DAC) produces a parametric time signal (ATIME).

The coincidence discriminator generates one trigger pulse for a each single event or a sequence of two pulses when a event coincidence happens. The buffered output (DIGOUT) of this signal is connected to the digitiser trigger input. If a coincidence in time of HOLD1 (GIPULSE, 1 μs width) and TP (TPULSE, 1 μs) happens, two trigger pulses within an interval of 1μs are generated, and for each one the multiplexer selects (through ASEL and PILE) the corresponding analog signal: AGI, ATIME or 0V.

The power present detector provides remotely readable control signals indicating the module's operational state.

The mixed analog-digital design and asynchronous nature of this circuit has implied a careful design of the analog block, specially on the printed circuit and power supply decoupling, in order to suppress the digital noise and guaranteeing the specified voltage resolution.

4. IMPLEMENTATION ON THE TCV TOKAMAK

The diode cryostat forced a horizontal mounting on an equatorial TCV port (Fig. 4). In the inherently "noisy" electrical environment of a fusion experiment, the diode, vacuum pumps and tokamak were all separately earthed and the electrical signal and power cables bundled together to minimise the effect of fluctuating magnetic

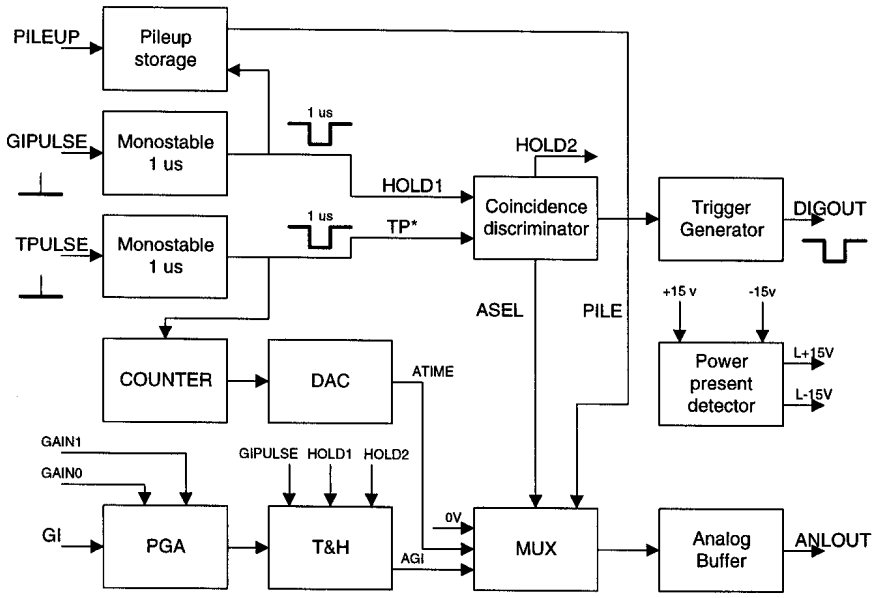

Fig. 3. Block diagram of the IATG unit.

fields. The diode was mechanically coupled via a high vacuum flight line (< 10^{-7} torr) to a TCV port which holds the possibility of externally change the viewing aperture and the introduction of Be filters into the flight line. For calibration purposes, it is also possible to place a Fe^{55} 5.9 keV radioactive source in one of the filter positions. A pair of apertures with 0.3 mm diameter at each end of the flight tube limits the atendue of the detector to the plasma to $1.2x10^{-6}$ Str m^{-2} in order to set a maximum observed count rate of 100 kHz in L-mode discharges.

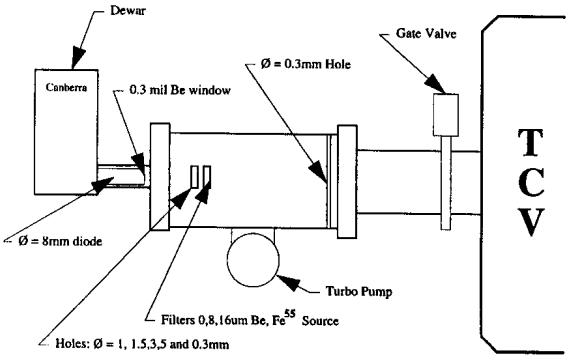

Fig. 4. Schematic view of the diagnostic.

5. RESULTS

The experimental results have shown that energy resolved spectra can be obtained during a TCV discharge. The values of the electron temperature are in good agreement with those determined with other diagnostics.

Fig. 5 shows the evolution of the electron temperature during a TCV discharge.

Another paper [4] presents the detailed studies of the influence of the apertures, Be filters and pulse pileup on the observed count rate and spectral shape. We have concluded that the maximum count rate is currently limited by the analog signal processing electronics.

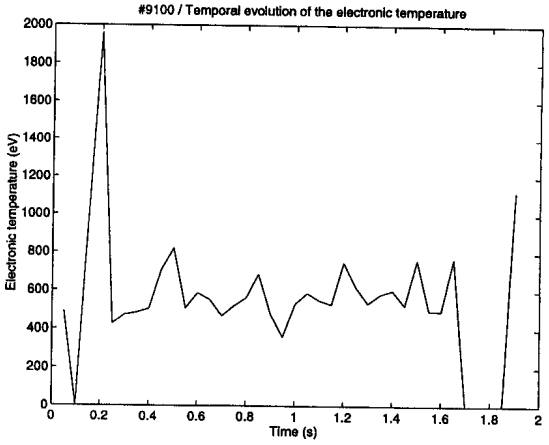

Fig. 5. Evolution of the electron temperature during a TCV discharge.

6. CONCLUSIONS AND FUTURE ENHANCEMENTS

An energy dispersive diagnostic has been successfully mounted on TCV for the analysis of the X-ray emission from a variety of plasma configurations. The interface amplifier and timing generator unit has allowed time resolved measurements of the electron temperature.

Future enhancements are needed in the analog electronic aiming at improving its operation in the electrically noisy TCV environment and to solve the pileup problems that presently limit the operation of this diagnostic.

REFERENCES

1. I. Hutchinson (1987). "Principles of Plasma Diagnostics", Cambridge University Press.
2. F. Hoffman et al (1994). Plasma Physics Controlled Fusion, B36, 277.
3. H. Weisen et al (1996). Plasma Physics Controlled Fusion.
4. B. P. Duval et al. Proceedings of the X-Ray spectroscopy conference, Lisbon 1996.

DESIGN AND INSTALLATION OF THE ELECTRON CYCLOTRON WAVE SYSTEM FOR THE TCV TOKAMAK

T.P. Goodman, S. Alberti, M.A. Henderson, A. Pochelon, M.Q. Tran

Association Euratom-Confédération Suisse, Ecole Polytechnique Fédérale de Lausanne, Centre de Recherches en Physique des Plasmas, 1015 Lausanne, Switzerland

The design of the combined 82.7 GHz and 118 GHz, 4.5 MW, 2.0 s electron cyclotron wave (ECW) system for heating and current drive on TCV is described. Low and high power test results of the RF source, transmission line and launching antenna are presented.

1. INTRODUCTION

The Tokamak à Configuration Variable (TCV) will require additional heating and plasma current profiling for the formation and study of strongly shaped plasma configurations. Highly-elongated ($\kappa \leq 3$) plasmas allow third harmonic X-mode (X3) heating to be used since power can be injected quasi-vertically along the resonance resulting in an increase in the optical depth of the plasma and good first pass absorption[1]. X3 enables higher central densities to be reached than with second harmonic heating (X2). Nevertheless, X2 is necessary for higher first pass absorption early in the discharge, when the elongation (X3 path length) is small, in order to shape the current profile and provide stable operation while elongating up to $\kappa=3$. In addition, the elongation evolution can be followed during the pulse.

The following paragraphs describe the design of a flexible, electron cyclotron current-drive/heating system with emphasis placed on the installation and testing of subsystems.

2. SYSTEM OVERVIEW

A total RF power of *4.5 MW* will be available during the *2 s* flattop of the TCV pulse; provided by nine *0.5 MW* gyrotrons grouped into three clusters of three units each. Each cluster is fed by one regulated high-voltage power supply (RHVPS) operating with pulse-step modulation technology[2]. Two of the clusters operate near the second harmonic (*82.7 GHz*) and one near the third harmonic (*118 GHz*). The frequencies are determined by the nominal magnetic field of TCV (*1.43 T*) and the availability of gyrotron sources. Although the frequency ratio of $X2/X3 \neq 2/3$, simultaneous central heating at both frequencies is still possible[3]. Each gyrotron RF beam is coupled to an evacuated transmission line via a "matching optics unit" (MOU) and propagated to a quasi-optical launching antenna installed on the tokamak.

2.1 Gyrotrons

Gyrotrons are delivered by Gycom (Russia) at *82.7 GHz* and Thomson Tube Electronics (France) at *118 GHz*. The RF window of the X2 gyrotron has a flattened power density profile on an edge-cooled boron nitride (BN) window while the X3 gyrotron has a gaussian profile on a liquid-nitrogen (LN) edge-cooled sapphire window. Neither window option is desirable at the torus. To avoid the problems associated with either readapting the beam profile or LN cooling at the tokamak, a windowless evacuated transmission line and MOU have been chosen.

2.2 MOU

The gyrotron RF beam contains scattered radiation that needs to be filtered before injection into the waveguide (to prevent arcing). The exact direction and position of the beam at the gyrotron window are not easily controlled during manufacturing within the precision nec-

essary for coupling to the transmission line; therefore, the alignment between the gyrotron and waveguide must be adjustable. Furthermore, the beam waist diameter and location must be modified to provide a proper match to the chosen waveguide diameter. The MOU serves these three functions (filtering, alignment and matching).

To provide optimum coupling of the transmitted RF beam to a given target plasma, the polarisation of the radiation must be adjusted: the MOU is a convenient location to perform this adjustment. To this end, a rotatable two-mirror universal polariser (Al) [4] is included in the MOU of the X2 gyrotron; along with two focusing mirrors (OFHC Cu) used to match the beam to the waveguide (Fig. 1). The four mirrors are aligned before evacuating the MOU and only the rotation of the polariser mirrors is possible under vacuum (between shots). All mirrors are cooled by conduction to the vacuum vessel walls.

The power that is lost in the MOU is absorbed by TiO_2-coated OFHC-Cu plates (*40% TiO_2 / 60% Al_2O_3, 0.3 mm* thick with an additional *0.08 mm* thick bonding layer) which are screwed onto rails welded to the vacuum vessel inner wall. The absorption of the plates has been measured at *45°* incidence in both the E and H-planes as *34%* and *18%*, respectively. The rather moderate absorption helps avoid hot spots.

The X3 MOU contains three water-cooled

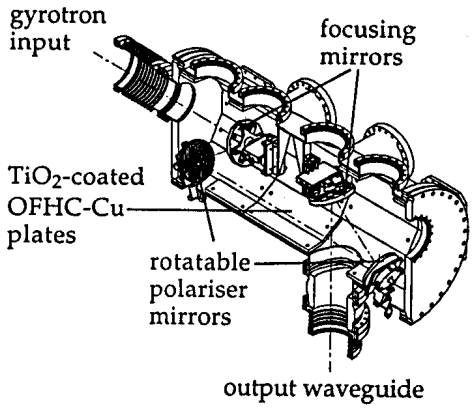

Figure 1. Evacuated MOU box of the X2 gyrotron.

mirrors (one focusing, and a two-mirror polariser) providing X-mode launch after propagation to the torus. The mirrors can be positioned while the MOU is evacuated.

2.3 Transmission lines

Corrugated HE_{11}-waveguide transmission lines (Al, *63.5 mm* diameter) have been procured from Spinner GmbH (Germany)/General Atomics (USA) and were delivered clean and ready for installation. The lines are bakable to *150 °C*.

A typical line is shown in figure 2. Electrical isolation breaks *(1)* are used to isolate the line from both the gyrotron/MOU and TCV. Miter bends *(2)* act as the fixed points of refer-

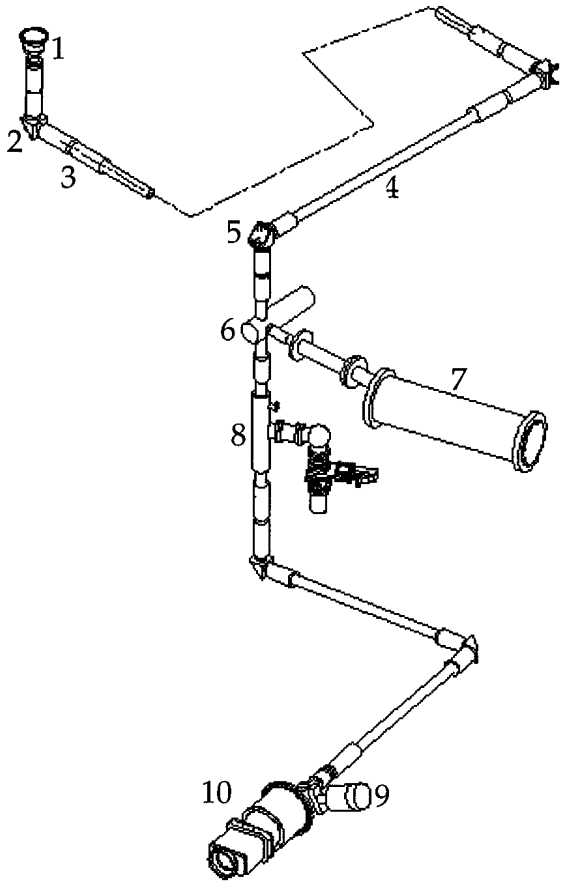

Figure 2. Typical transmission line for X2 gyrotrons. The average length of the lines is approximately *30 m*.

ence for support and alignment. Additional adjustable supports are placed along the lines ~ *3 m* apart. They are laser aligned with the miter bends and constrain the line only in the vertical direction to avoid excess gravitational sagging. Each corrugated bellows *(3)* provides *5 mm* extension and *30 mm* compression to compensate for thermal expansion and waveguide length tolerances. Straight sections *(4)* are as long as possible (*2.1 m*) to minimize the total number of joints (potential misalignments) and Helicoflex® vacuum seals (potential leaks). Forward and reflected power signals are provided by a power monitor miter bend with multihole coupling *(5)*, placed as near TCV as possible while still allowing *in situ* calibration against a calorimetric load. A switch *(6)*, with integral gate valves on the outputs, directs the power to either the torus or a stainless steel water-cooled load *(7)* fitted with flow and temperature probes for calorimetric measurements and a small vacuum port for pressure measurements and pumping. To minimize impurity throughput to the plasma, a pumping "tee" *(8)* is located near the torus. An all-metal gate-valve *(9)* separates the launching-antenna vacuum chamber *(10)* (at torus pressure) from the transmission line.

The bellows of the last and next to the last legs of the transmission line compensate for TCV expansion (*~7 mm* vertically and horizontally) during baking (*300* °C). From the torus to the first vertical bellows, the line is kept as simple as possible to ease vertical motion. The last leg can easily be removed to allow access to the launching antenna while maintaining the vacuum from the MOU to the switch; and can be evacuated by the pumping "tee" after reinstallation.

The majority of the line (MOU → load) can be tested under vacuum at high power and long pulse length, independently from TCV.

2.4 Launching antennas

Rectangular boxes (*15x36x36 cm*) extending beyond the TCV shaping coils are welded onto the torus at six entry ports of *15 cm* diameter (four upper lateral and two equatorial). Upper lateral ports are *45.5 cm* above the equatorial (mid-) plane and *28 cm* outward along the major radius. Thus, to be able to aim centrally toward the midplane (downwards), it is necessary to have the final reflection point of the beam located inside the circular port itself. To maintain good localization of the beam, focusing is required between the end of the transmission line and the plasma.

Each X2 launching antenna (Fig. 3) has the capability of aiming in the poloidal and toroidal directions to cover X-mode heating, current profile modification, current drive and breakdown. The last mirror of the four-mirror antenna can be moved over a *24°* range, twice, during a discharge, while the entire antenna can be rotated *0–360°* about the axis of the port between shots: virtually the entire poloidal cross-section can be targeted. The first three mirrors of the antenna are made of OFHC-Cu with the first and third providing focusing. The fourth mirror is made of TZM (a machinable alloy of *Mo: 0.02% C, 0.5% Ti, 0.1% Zr, 99.25% Mo*) due to the mirror's proximity to

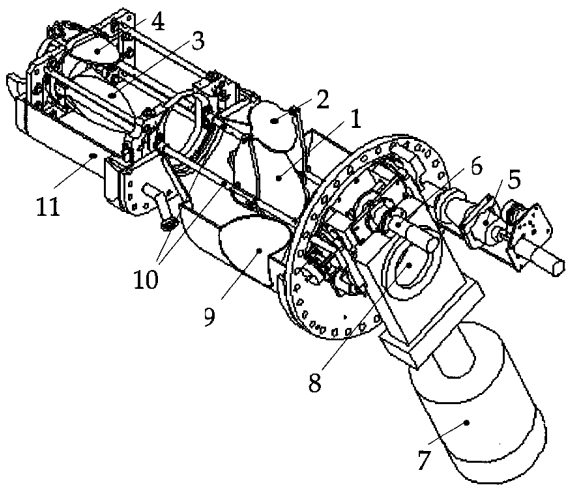

Figure 3. Elements of the X2 4-mirror launching antenna: mirrors *(1-4)*, rotational feedthrough *(5)*, linear actuation system of mirror 4 *(6)*, all-metal gate valve *(7)*, RF input *(8)*, indentation in vacuum vessel to avoid hitting TCV support structure *(9)*, guiding tubes of 4th-mirror actuator rods *(10)*, rectangular box *(11)* welded to the circular TCV entry port.

the plasma. Molybdenum has relatively low sputtering, low thermal expansion, high melting point and reasonably high thermal and electrical conductivity (peak $\Delta T \sim 470°C$, at 0.3% duty cycle: average $\Delta T \sim 110°C$ assuming only radiative cooling).

X3 power will be launched from one port on the top of the machine. All three RF beams are directed onto a single mirror focusing in the poloidal direction only. The beams can be directed, as a group, in the poloidal plane by changing the mirror angle during a shot. The mirror location along the TCV major radius can be varied between shots to optimise first-pass absorption and avoid resonances on the mirror.

3. TEST RESULTS

One X2 gyrotron has been accepted at present, having been tested at *>0.5 MW, 2s, 1% duty cycle* for *4 hours* without missing any shots. Two further gyrotrons have been delivered and are presently under test. The prototype X3 gyrotron is undergoing factory tests [5].

The first three transmission lines have been delivered and most legs of the first cluster have been installed and pumped. One line (*4 miterbends, 20.1m*) has undergone vacuum testing using a *500l/s* turbopump at the MOU; resulting in a pressure of 1.0×10^{-7} *mbar* at the MOU, 3.5×10^{-6} *mbar* at the end of the line and an outgassing rate of 1.1×10^{-11} $mbar \cdot l \cdot s^{-1} \cdot cm^{-3}$. The calculated conductance of the corrugated waveguide is $\sim 0.36\ l \cdot s^{-1}$ (~2.4 times lower than for smooth waveguide) yielding a pressure difference of 3.3×10^{-6} *mbar* for the above outgassing rate; in close agreement with the measurements.

The accepted X2 gyrotron was connected to the transmission line (without antenna) and tested at atmospheric pressure. Burn patterns after the MOU and at the output of the line show a well centered beam with some mode impurity. Pulses of *0.1s* and *0.5 MW* - measured at both the end of the transmission line and after the switch – were achieved without arcing. The power monitor miter bend was calibrated against the *100 ms* - calorimetric load used for the acceptance tests of the gyrotron. The coupling is found to be *-87.0±0.2dB* . The measured line efficiency (P_{input}/P_{output}) is *93±5%*. A flat alignment mirror (used in place of the polariser grating) was rotated to check the alignment properties of the MOU: no systematic power variation was seen.

High power long pulse conditioning tests have also begun. At present, a maximum of *0.6 MJ* (*309kW* for *2.0s* or *405kW* for *1.6s.*) has been transmitted - limited by the large pressure rise seen in the unbaked MOU.

Three X2 launching antennas have been tested (low-power RF; vacuum, mechanical at *150°C*) confirming all the design parameters.

4. CONCLUSION

Initial TCV ECW system tests have begun. Three launchers are now installed and tests with ECW power in TCV are planned for this fall.

ACKNOWLEDGMENTS

The authors would like to thank Dr. J. Doane (General Atomics) for his transmission line calculations and many helpful discussions. The participation of Dr. I. Roy (Kurchatov Institute) during part of the high power tests is gratefully acknowledged. Special thanks go to the drafting, electrical, electronics and vacuum departments of the CRPP for their invaluable support. This work is partially supported by the Swiss National Science Foundation.

REFERENCES

1. Ségui J. L. et al., Nucl. Fusion, 1996, **36**, 237.
2. Fasel D. et al., "Design and operation of the power installation for the TCV ECR additional heating", this conference.
3. Pochelon A. et al., in Proceedings of the 20th EPS Conf. on Controlled Fusion and Plasma Physics, Lisboa, Portugal, 1993, Vol. 17c Part III, 1020.
4. Smits F. M. A. in Proceedings of the 7th Joint Workshop on ECE and ECRH (Heifei, China) 1989.
5. M. Pain et al., this conference.